Generic dimer-buckling model for semiconductor surfaces: Dynamical simulations

Dorothea K. Stillinger and Frank H. Stillinger
AT&T Bell Laboratories, Murray Hill, New Jersey 07974
(Received 28 June 1993)

Molecular-dynamics simulation has been employed to investigate a previously proposed statistical-mechanical model [F. H. Stillinger, Phys. Rev. B **46**, 9590 (1992)] for dimer buckling on the reconstructed Si(001) surface. Using model parameters suggested by low-temperature scanning-tunneling-microscopy observations, the calculations reveal a weakly first-order phase transition from a low-temperature $c(4\times2)$ pattern of buckled dimers, to a disordered high-temperature phase in which dimers have the untipped state as their most probable configuration. Alterations of input parameters establish that the thermal behavior of the generic model is sensitive to their specific values. Cases of strong first-order and of higher-order (Ising-like) phase transitions have also been simulated, as well as a case devoid of transitions.

I. INTRODUCTION

A conceptually simple model was recently introduced[1] to describe the cooperative buckling (tipping) of surface dimers on semiconductor crystals. This development occurred in response to a long and contentious history of experimental[2–8] and theoretical[9–15] studies devoted to the existence and status of dimers, specifically on the Si(001) surface. Analogous dimerization has also been observed on Ge(001),[16,17] and for Ge monolayers deposited on Si(001).[18,19]

Wolkow's recent low-temperature (120 K) scanning-tunneling-microscopy (STM) images of the dimerized Si(001) surface[8] have been interpreted[1] as suggesting that both buckled and unbuckled dimer patterns separately possess mechanical stability, but that the former attains the lowest possible energy by adopting a $c(4\times2)$ pattern. The generic model defined in Ref. 1 exhibits such behavior with the proper choice of parameters. However, it has heretofore remained an open question whether the existence of such ordered buckling patterns is associated with a strict (i.e., thermally sharp) surface order-disorder phase transition. The purpose of the present paper is to investigate the phase transition behavior of the generic buckling model, using the molecular-dynamics simulation technique, to see in principle what possibilities exist.

The following Sec. II outlines our model. The simulation protocols appear in Sec. III. Rather detailed simulation results are presented in Sec. IV for a "standard" choice for the four parameters appearing in the model; this choice may be a reasonable set for the Si(001) applications but may need modification for Ge(001).[20] Alternative parameter sets are briefly considered in Sec. V to provide a more comprehensive view of the phase transition richness inherent in the generic model, which viewed from the conventional statistical-mechanical perspective is a bit unorthodox. Section VI takes up the issue of assigning dimensions and units to the model to permit direct comparison with experiments and other theoretical calculations. Finally, Sec. VII offers some discussion and summarizes conclusions.

II. MODEL

Figure 1 illustrates schematically the rectangular array of surface dimers on Si(001) in the symmetric untipped (unbuckled) state, and after tipping (buckling) to produce the $c(4\times2)$ pattern that presumably minimizes the energy. We suppose that dimer i can be described by a single angle variable α_i that vanishes in the untipped configuration. Our model amounts to a proposed form for $\Phi(\alpha_1\cdots\alpha_N)$, the potential-energy function for an arbitrary set of buckling angles for the N dimers.

For present purposes we will suppose that the dimer system is defect-free (however, see Ref. 1 for a proposed coupling to surface defects).

The general form assigned to Φ is as follows:[1]

$$\Phi=\sum_{i=1}^{N} f(\alpha_i,B_i)+\Phi_{\rm int}\ , \tag{2.1}$$

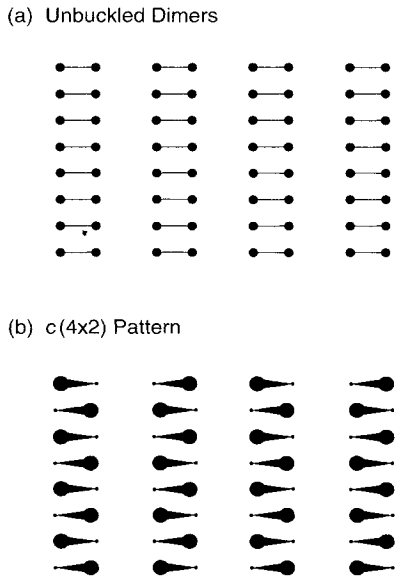

FIG. 1. Schematic views, from above, of dimers on the reconstructed Si(001) surface.

where

$$f(\alpha,B)=\alpha^4+B\alpha^2 \tag{2.2}$$

plays the role of an effective single-dimer buckling potential, and where Φ_{int} represents interactions between nearby dimers. Experiments suggest a strong buckling-sense anticorrelation along the columns indicated in Fig. 1, and a weaker anticorrelation in the other surface direction. This feature is accommodated in the model by anisotropy in Φ_{int}.

The present study has considered only the case of nearest-neighbor interactions in Φ_{int}. Hence we take (with $J,\varepsilon\geq 0$)

$$\Phi_{\text{int}}=\tfrac{1}{2}J\left[(1-\varepsilon)\sum_{\text{column}}\alpha_i\alpha_j+\varepsilon\sum_{\text{row}}\alpha_k\alpha_l\right], \tag{2.3}$$

where the indicated sums respectively include (once) each nearest-neighbor pair along the columns and along the rows. The observed anisotropy requires $0<\varepsilon<\frac{1}{2}$.

The effective single-dimer potential f, Eq. (2.2), has a single minimum, at $\alpha=0$, if $B\geq 0$. However, it becomes a bistable potential for $B<0$ with minima displaced symmetrically from the origin. A fundamental characteristic of our generic model is that both cases are permitted to occur, depending on the status of the neighboring dimers. It is by this means that both buckled and unbuckled patterns of surface dimers can possess mechanical stability. Utilizing two more positive parameters K and λ, B_i has been assigned the form

$$B_i=-2+\tfrac{1}{2}K\left[(1-\varepsilon)\sum_{\text{column}}(\alpha_j^2-\lambda^2)^2+\varepsilon\sum_{\text{row}}(\alpha_k^2-\lambda^2)^2\right], \tag{2.4}$$

which incorporates the same column-row anisotropy as in Φ_{int}. Because B_i refers to a single dimer i, each of the two sums in Eq. (2.4) contains only a pair of terms: the two nearest neighbors in the same column for the first, and the two nearest neighbors from flanking columns in the second.

If the four neighbors of dimer i all were tipped to angles $\pm\lambda$, B_i would reduce to -2. In this circumstance the effective single-dimer potential $f(\alpha_i,-2)$ would have minima of depth -1 at $\alpha_i=\pm 1$. Any deviations of the four neighbors' angles from $\pm\lambda$ cause B_i to rise above -2, and eventually to become positive. While the B_i influence the buckling of dimers, they do not distinguish between same-sense and opposite-sense buckling of neighbors.

The expressions (2.3) for Φ_{int} and (2.4) for B_i cause the full potential Φ to be a sixth-order multinomial in the angle variables $\alpha_1\cdots\alpha_N$. It is easy to show that Φ possesses the necessary symmetry and stability requirements, and leads in the large system limit to proper thermodynamic behavior. Four non-negative parameters J,K,ε, and λ appear in Φ, whose magnitudes we shall see below strongly influence phase transition behavior of the model.

III. DYNAMICAL SIMULATION PROCEDURE

Our dynamical simulations were carried out for an array of $N=240$ dimers located in ten columns, each of 24 dimers. Periodic boundary conditions applied in both surface directions. Time evolution was described by Newton's classical equations of motion that correspond to the assumed reduced Hamiltonian function:

$$H^*=\tfrac{1}{2}\sum_{i=1}^{N}\dot{\alpha}_1^2+\Phi(\alpha_1\cdots\alpha_N)\,, \tag{3.1}$$

with potential Φ having the form specified in Sec. II. Units have been chosen in Eq. (3.1) to make the effective mass equal to unity for each angular degree of freedom. For all of the calculations described below the equations of motion,

$$\ddot{\alpha}_i=-\frac{\partial\Phi}{\partial\alpha_i}\quad(i=1\cdots N)\,, \tag{3.2}$$

were numerically integrated using the sixth-order Gear algorithm[21] with a time increment (in reduced units) of 0.002 to respect energy conservation to high precision.

The bulk of our calculations utilized the following "standard" parameter set ("case 1"):

$$J=2.2,\quad K=1.0,\quad \varepsilon=0.11,\quad \lambda=1.6\,; \tag{3.3}$$

this was identified in the prior paper[1] as appropriate (roughly) for description of the Si(001) case, at least as judged by the available low-temperature STM observations.[2] Three other contrasting cases have also been studied; they correspond, respectively, to setting $J=0$, to $K=0$, and to $\varepsilon=0.5$, but in each case keeping the other three parameters at the case 1 values shown in Eq. (3.3).

Molecular-dynamics production-run sequences followed a uniform protocol for all four cases. Starting at low temperature, pairs of runs at the same total energy were generated: the first (for equilibration) spanned 4×10^4 dynamical steps, the second (to provide statistical averages) spanned 2×10^5 dynamical steps. Both heating and cooling sequences were produced to check for hysteresis effects, particularly in phase transition regions. The former involved momentum scale factor 1.02 at the beginning of each equilibration run, while the latter involved scale factor 0.98.

IV. SIMULATION RESULTS, "STANDARD" PARAMETER SET

Figure 2 presents the mean potential energy per dimer, $\langle\Phi\rangle/N$, versus reduced temperature,

$$T^*=\left\langle N^{-1}\sum_{i=1}^{N}(\dot{\alpha}_i)^2\right\rangle, \tag{4.1}$$

for the standard parameter set in Eq. (3.3). The data shown emerged from a cooling sequence as specified in the preceding Sec. III. A very similar curve has been produced by an analogous heating sequence.

The nearly vertical rise appearing in Fig. 2 is the striking signature of a phase transition. In fact we identify this behavior as a weakly first-order transition accom-

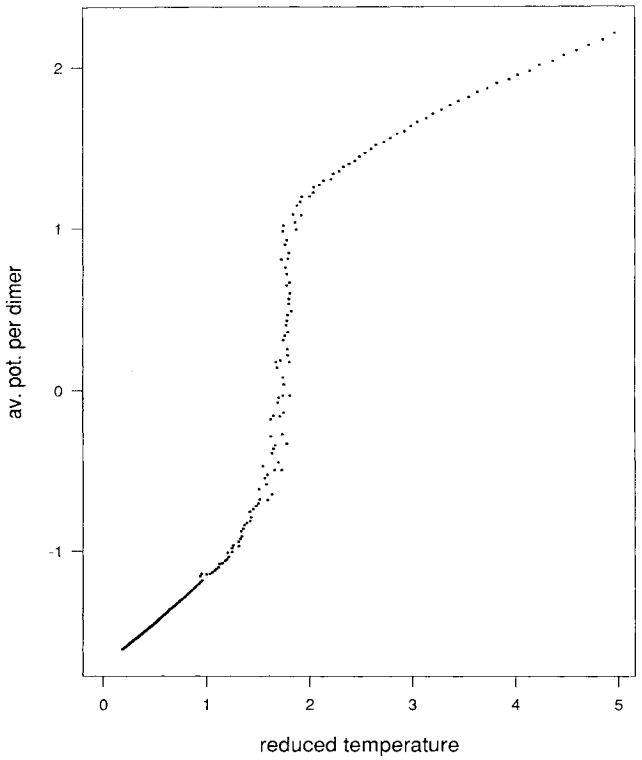

FIG. 2. Mean potential energy per dimer vs reduced temperature, for the standard "case 1" set of model parameters. These data were generated during a molecular-dynamics cooling sequence.

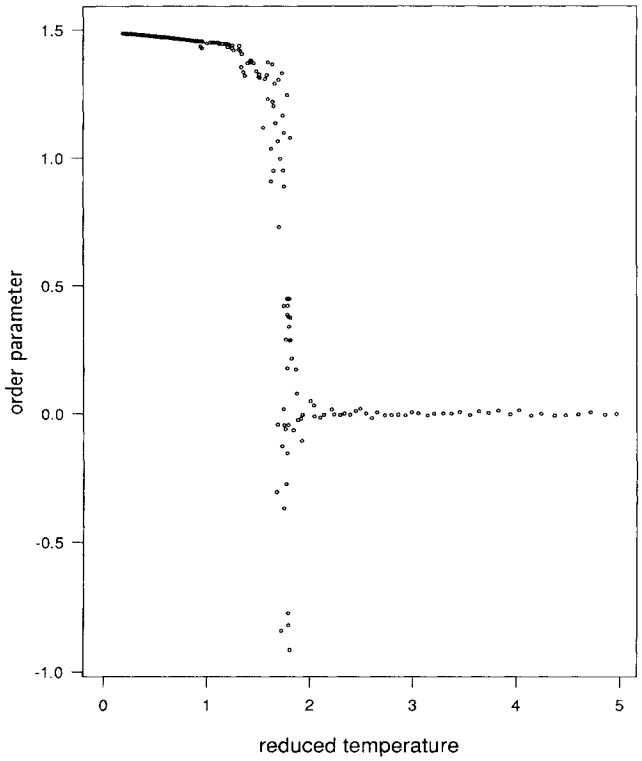

FIG. 3. Long-range order parameter vs reduced temperature during a case 1 cooling sequence.

panied on the low-temperature side by a substantial "premelting" phenomenon. The data shown convey a slight sigmoid shape due to a very small extent of supercooling prior to phase transition. We estimate that the implied thermodynamic melting transition in the infinite system limit would occur at

$$T_m^* = 1.80 \ . \tag{4.2}$$

The natural long-range order parameter for the system is the following intensive quantity:

$$R = N^{-1} \sum_{x,y} (-1)^{x+y} \alpha(x,y) \ , \tag{4.3}$$

where x and y are integer indices locating the dimer on the surface. In the fully ordered ground state with the standard interaction set (3.3), the angles alternate between values $\pm 1.493\,51$, so R must lock onto one of these values as T^* goes to zero.

Figure 3 shows $R(T^*)$, evaluated during the same cooling sequence that yielded Fig. 2. The tipping angles are fully disordered above T_m^*, and so R vanishes in this high-temperature regime. But the phase transition suddenly orders the dimers in the expected alternating pattern as T^* falls below T_m^*, and indeed R approaches $+1.493\,51$ in the low-temperature limit. Linear deviations from this value at low, but positive, T^* are the result of vibrational motions.

That the system chose the positive R branch at T_m^* was a matter of pure chance. Other cooling simulations have spontaneously selected the negative R branch. It is clear from Fig. 3 that strong configurational fluctuations occur near the phase transition point, temporarily driving the long-range order parameter to negative values.

The distribution of tipping undergoes a dramatic change in character as the system passes through the phase transition. Figures 4–6 provide illustrations from another cooling sequence (virtually identical behavior has been obtained during heating). The first of these, Fig. 4, shows the distribution in the ordered state at $T^* = 1.464$, well below the "melting" transition. As expected, the distribution is symmetric but vividly bimodal, with peaks located near the $T^* = 0$ values mentioned above. Clearly each dimer experiences an effective bistable function f, Eq. (2.2). If separate sublattices in this ordered state were to have been distinguished, each would have displayed just one of the two peaks appearing in Fig. 3; we have chosen to combine them. At the given temperature the dimer vibrations are sufficiently anharmonic to produce perceptible skewing of the peaks toward zero angle, but at lower temperature this skewness disappears as the separate peaks narrow.

Figure 5 displays the drastically different angle distribution that obtains in the disordered state at $T^* = 2.388$. Now the distribution has become unimodal, but broad and with distinct shoulders in the ranges, roughly, of the $T^* = 0$ tipping angles.

Figure 6 indicates the result of yet a further rise in temperature, to $T^* = 4.917$. While the distribution con-

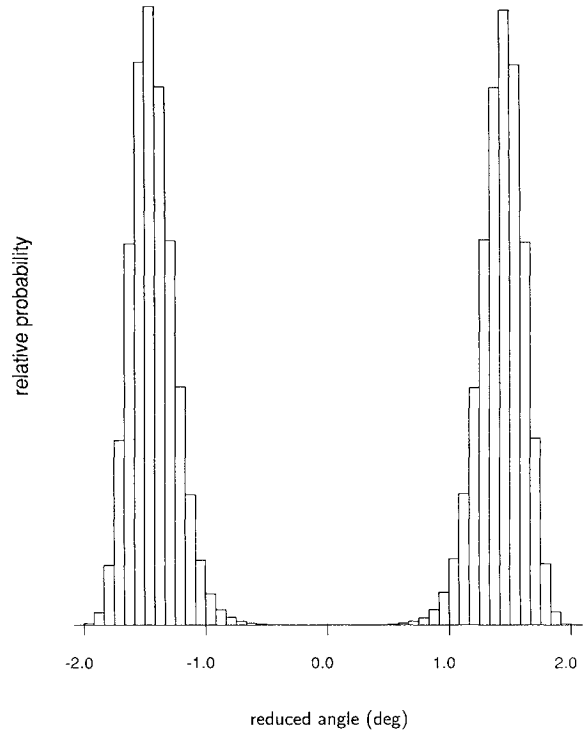

FIG. 4. Angle distribution for case 1 in its ordered state at $T^* = 1.464$.

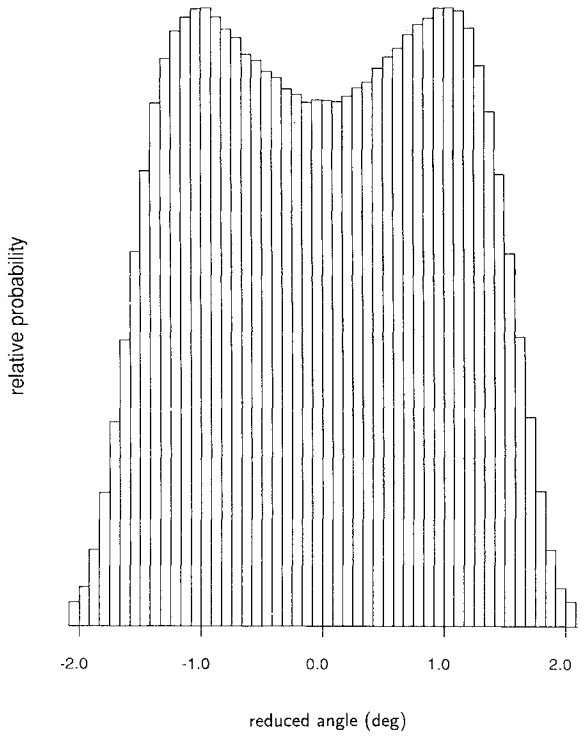

FIG. 6. Angle distribution function for case 1 in the disordered state at $T^* = 4.917$.

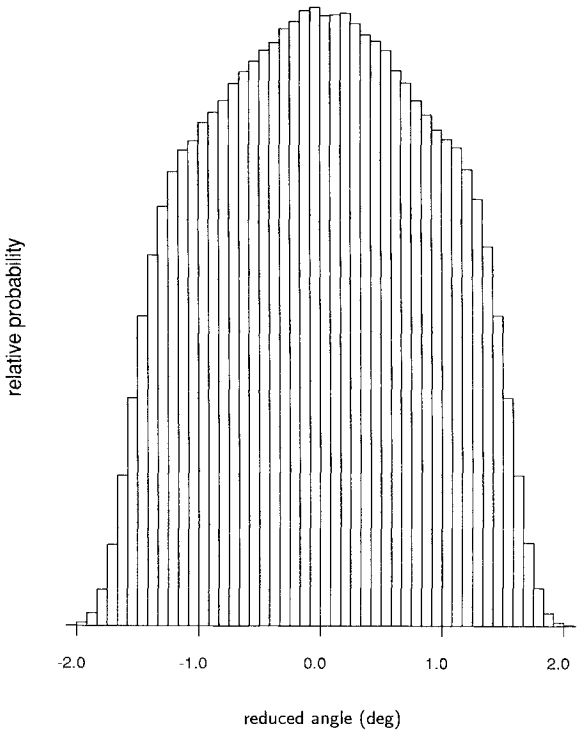

FIG. 5. Angle distribution for case 1 in the disordered state at $T^* = 2.388$.

tinues to be broad, it has surprisingly returned to bimodality, though only weakly so. Of course this is not the result of a return to an ordered state, but of substantially increased vibrational amplitudes that frequently drive the $|\alpha_i|$ to the neighborhood of $\lambda = 1.6$, and consequently permit the B_i in Eq. (2.4) occasionally to adopt strongly negative values.

Identification of "inherent structures" (i.e., potential-energy minima) during cluster[22–24] and condensed phase[25–29] simulations has often been an important source of physical insight. Presuming the same may be the case for surface phenomena, we have examined inherent structures for the present model, utilizing randomly chosen (but presumably typical) system configurations from the simulations as starting points. Given any such initial configuration, a steepest-descent relaxation is then carried out on the Φ hypersurface in the full space of tipping angles to identify the relevant local (or global) Φ minimum.

When the dimer system is in the low-temperature ordered phase, the steepest-descent mapping simply recovers the global minimum, one of the two degenerate alternating patterns of angles $\pm 1.493\,51$. The only effect of reduction to the inherent structure is to remove vibrational excursions of the dimer angles from these fiducial values.

Inherent structures obtained by steepest-descent mapping from the disordered high-temperature phase correspond to higher-lying Φ local minima. The corresponding sets of tipping angles show characteristic patterns

with columns of dimers (see Fig. 1) in either of two states. Approximately one-quarter of the columns consist of dimers all of which are substantially untipped. The remaining columns have all their dimers tipped at roughly the fiducial values $\pm 1.493\,51$; while these are significantly anticorrelated from one to the next, blocks of one or more within the column will frequently have reversed sign.

The time scale of configurational fluctuations controls the behavior of the tipping angle correlation function:

$$A(t)=\langle \alpha_i(t_0)\alpha_i(t_0+t)\rangle \ , \tag{4.4}$$

which at equilibrium will be independent of dimer index i and time t_0. Figures 7 and 8, respectively, show the initial portions of $A(t)$ for a low-temperature ordered state ($T^*=0.944$) and a high-temperature disordered state ($T^*=2.271$). The low-temperature behavior shown in Fig. 7 is highly oscillatory, but only involves small-amplitude, essentially harmonic, dimer vibrations about the value dictated by the long-range order R for that temperature. The result in Fig. 8 has quite a different appearance, decaying to zero, albeit with slight overshoot and rebound. The long positive tail in $A(t)$ for this latter case is probably connected to persistence of column-type patterns (tipped vs untipped) that were revealed by the high-temperature inherent structures discussed above. The time scales differ substantially for these two cases: the first $A(t)$ minimum occurs at reduced times $t^*=0.22$ and 0.93, respectively, for Figs. 7 and 8.

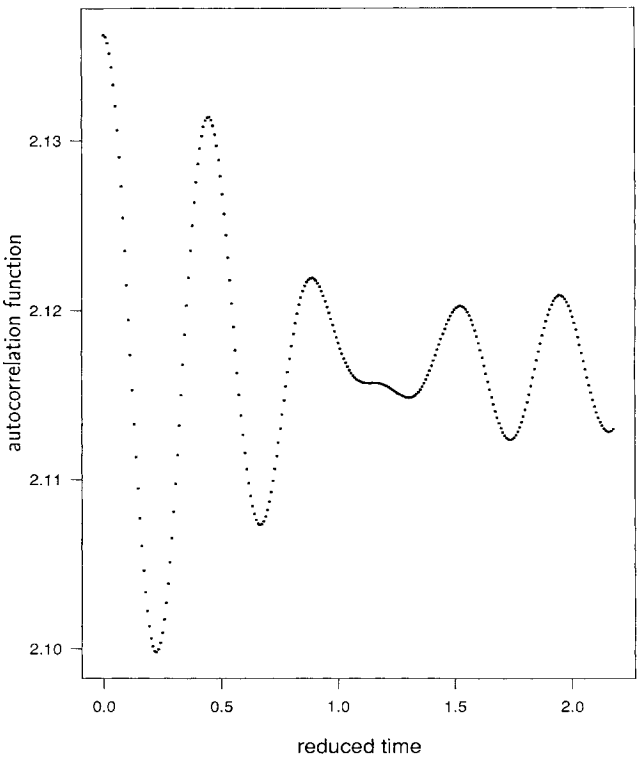

FIG. 7. Angle autocorrelation function vs reduced time for case 1 at $T^*=0.944$ (low-temperature ordered phase).

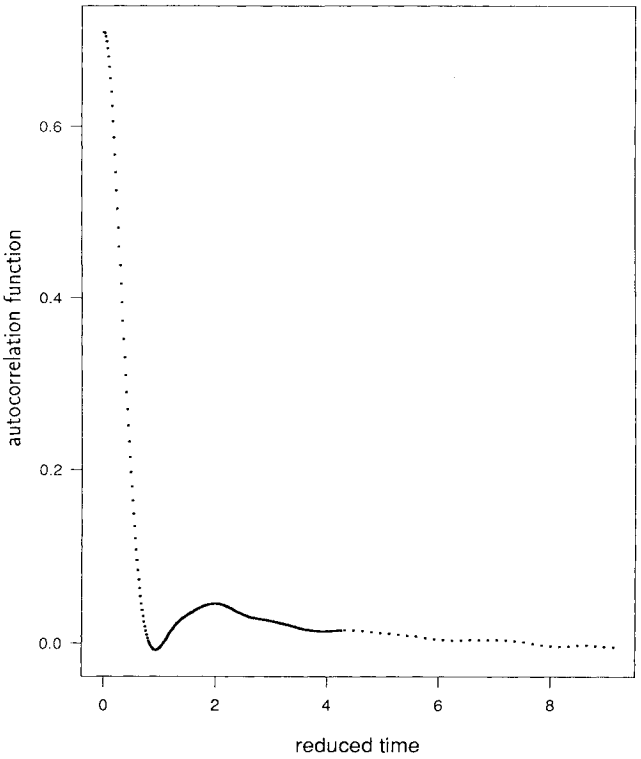

FIG. 8. Angle autocorrelation function vs reduced time for case 1 at $T^*=2.271$ (high-temperature disordered phase).

V. ALTERED PARAMETERS

In order to attain a more comprehensive understanding of the dimer-buckling model it has been useful to vary the basic parameters J,K,ε,λ from the standard set (case 1) shown in Eq. (3.3). Three other cases have been examined with molecular-dynamics simulation. Each differs from the standard set only by alteration of one of the parameters. Table I provides details.

Case 2 is obtained by setting $K=0$. This has the effect of pinning all B_i to the value -2, as Eq. (2.4) makes clear. Each dimer is then always subject to a bistable buckling potential $f(\alpha_i,-2)$ regardless of the state of tipping of its neighbors. The resulting invariable bimodality suggests that this case may be similar to the field-free two-dimensional Ising model, and indeed the simulation appears to show the presence of a critical tempera-

TABLE I. Parameter sets and transition characteristics.

	Case 1	Case 2	Case 3	Case 4
J	2.2	2.2	0.0	2.2
K	1.0	0.0	1.0	1.0
ε	0.11	0.11	0.11	0.5
λ	1.6	1.6	1.6	1.6
transition temperature	1.80	1.00	· · ·	1.80
transition order	1	>1	· · ·	1

ture and higher-order phase transition. Figure 9 shows the mean potential energy per dimer, and Fig. 10 the order parameter, both versus reduced temperature, during a cooling sequence (heating sequences have produced similar results). The former seems to be consistent with an Ising-like logarithmic heat capacity singularity at $T_c^* \cong 0.25$, and the latter with an Ising-like magnetization critical exponent $\beta = \frac{1}{8}$. However, our simulation system is too small and the running times too short to permit direct quantitative verification of these presumptions.

Case 3 differs from case 1 by having $J=0$. Neighboring spins still interact, though only through the bistability-controlling quantities B_i, Eq. (2.4). These residual interactions suffice to create inherent structures with stably tipped dimers; in particular any configuration with all $|\alpha_i| = 1.407\,16\ldots$ is a local Φ minimum. However, these 2^N degenerate inherent structures all lie substantially higher in Φ than the nondegenerate global minimum at $\alpha_1 = \alpha_2 = \cdots = \alpha_N = 0$, i.e., $\Phi/N = 0.626\,47\ldots$ vs 0.

Simulation indicates that no phase transition occurs for case 3. The mean potential energy per dimer rises smoothly with temperature, displaying no hint of a vertical tangent. The order parameter remains zero at all temperatures.

Case 4 is the isotropic version of case 1, obtained simply by setting $\varepsilon = 0.5$. Figures 11 and 12, respectively, exhibit the potential per dimer and the order parameter as functions of temperature. The data shown in this instance were generated during a heating sequence. Evidently making the interactions isotropic has converted the weakly first-order transition of case 1 to a significantly stronger first-order transition. Both Figs. 11 and 12 show obvious superheating of the ordered phase before melting. That a stronger first-order phase change is present receives support from the fact that cooling from high temperature at the standard rate used for all four cases fails to nucleate the ordered phase. Instead of freezing into the pattern of alternating tipped dimers required by equilibrium, the system supercools to $T^* = 0$, ending in the totally untipped configuration.

A reasonable estimate of the melting temperature for case 4 (the location of a vertical tie line in Fig. 11) is

$$T_m^* \cong 1.80 , \tag{5.1}$$

the same, within our precision, as for the anisotropic case 1. The jump discontinuity in potential energy per dimer is

$$\langle \Delta\Phi \rangle / N \cong 0.70 , \tag{5.2}$$

leading to the following estimate of the entropy change per dimer upon melting:

$$\Delta S / N k_B \cong 0.39 . \tag{5.3}$$

Results from the four simulation cases can be combined with a few general considerations to provide a more global view of the phase transition character of the dimer-buckling model. Figure 13 presents our tentative view of the J,K plane (first quadrant) with $\varepsilon = 0.11$, $\lambda = 1.6$, divided into regions according to the type of

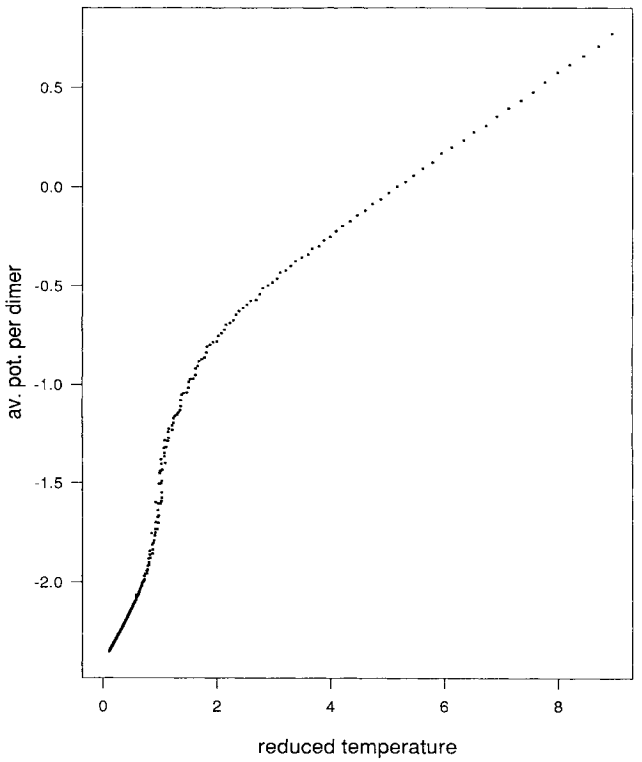

FIG. 9. Mean potential energy per dimer vs reduced temperature for the case 2 parameter set, generated during a cooling sequence.

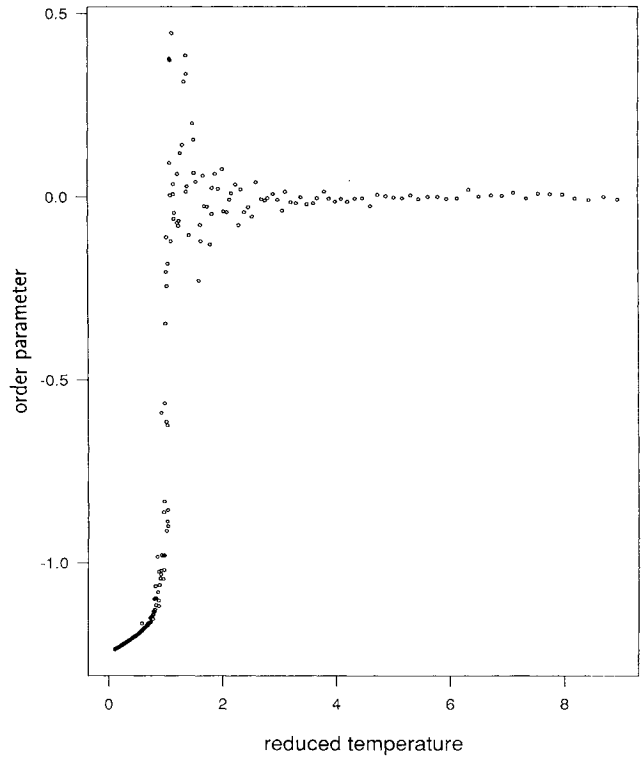

FIG. 10. Long-range order parameter vs reduced temperature for case 2 (cooling sequence).

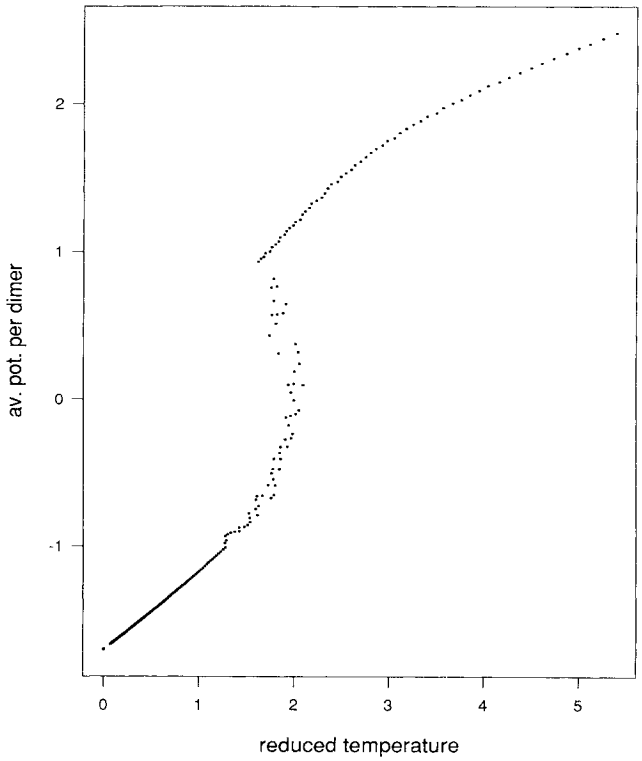

FIG. 11. Mean potential energy per dimer vs reduced temperature for case 4 (heating sequence).

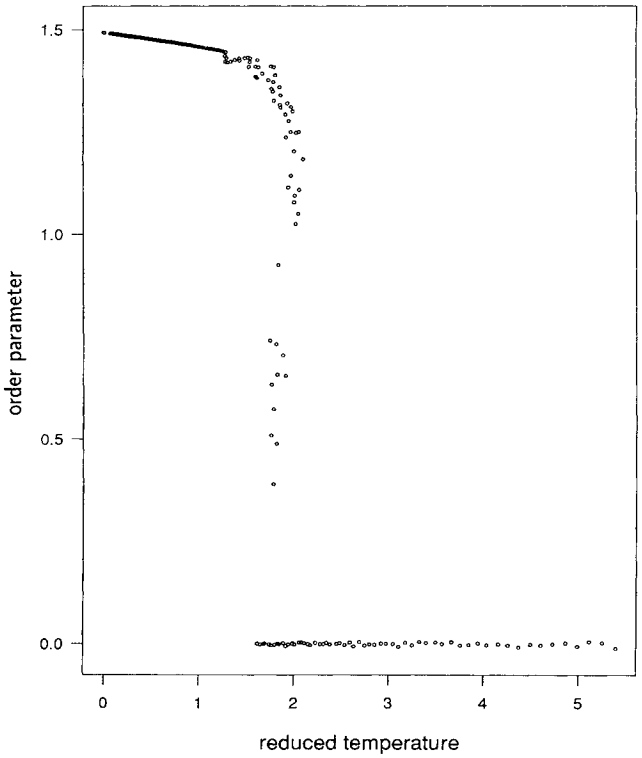

FIG. 12. Long-range order parameter vs reduced temperature for case 4 (heating sequence).

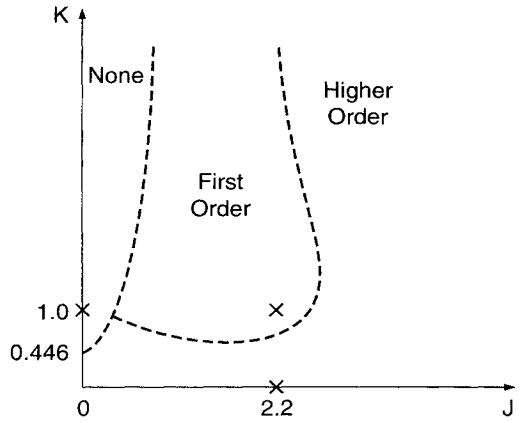

FIG. 13. Approximate partitioning, by phase transition type, of the first J,K quadrant for the dimer-buckling model with $\varepsilon=0.11$, $\lambda=1.6$.

phase transition expected (if any). This view has incorporated the following considerations.

(1) For sufficiently small (but nonzero) K the system should continue to fall in the field-free Ising universality class. Hence the higher-order phase transition region should contact the entire positive J axis.

(2) When $J=0$, the potential is insensitive to signs of the α_i as noted above in the discussion of case 3. To identify the ground state and possible instabilities, set all $\alpha_i=\alpha$, so the potential per dimer becomes

$$\Phi/N=K\alpha^6+(1-2K\lambda^2)\alpha^4+(K\lambda^4-2)\alpha^2 . \quad (5.4)$$

When $0\leq K<0.446$, this expression possesses a pair of negative minima at nonzero α. But when K passes through 0.446 these minima rise through zero, and are preempted by a zero-potential minimum at $\alpha=0$. A simple argument suggests that this crossover point should be associated with loss of the Ising-like phase transition. Beyond this point the remainder of the positive K axis should contact a "no transition" strip.

(3) If $K>0$ is held fixed, taking J to $+\infty$ asymptotically should always return to the Ising universality class [with the transition temperature increasing in proportion to $(J/K)^{1/4}$, asymptotically].

(4) In the $K\rightarrow+\infty$ asymptotic limit, the form of B_i requires either that all the α_i cluster closely around $\pm\lambda$, or that all cluster closely around zero. The value of J controls which of these types of inherent structures produces the lowest energy. If $J<2\lambda^2-4$ the latter yields the lower energy; for $J>2\lambda^2-4$ the former does. This should produce a finite range of J over which a first-order transition exists.

VI. ASSIGNMENT OF UNITS

The buckling model theory and molecular-dynamics calculations thus far have been presented entirely in dimensionless form. Contact with observations on the real Si(001) surface requires redimensioning the model. This involves identifying appropriate scale factors (units) for

time, energy, and tipping angle, to be denoted, respectively, by τ_0, ε_0, and θ_0.

Figure 14 provides a simple geometric picture of a tipping dimer which can serve as the basis for redimensioning. The view shown is along the surface, perpendicular to the dimer axis. As the dimer tips, its two silicon atoms (denoted by 1 and 2 in the diagram) remain in the plane of the drawing. For simplicity of interpretation we assume that (a) the dimer bond length l remains unchanged by tipping, (b) the projected bond lengths b of dimers to atoms in the layer below (actually an eclipsed pair of bonds) also remain unchanged during tipping, and (c) the projected positions P and Q of the substrate atoms remain fixed.

The actual dimer-tipping angle has been denoted by θ in Fig. 14. Elementary trigonometry shows that it is related to the angles ψ_1 and ψ_2 of the projected bonds at P and Q by

$$\sin\psi_2-\sin\psi_1=(l/b)\sin\theta \ . \tag{6.1}$$

To leading order in θ this implies

$$\begin{aligned}\psi_1&=\psi_0-l\theta/(2b\cos\psi_0) \ ,\\ \psi_2&=\psi_0+l\theta/(2b\cos\psi_0) \ ,\end{aligned} \tag{6.2}$$

where ψ_0 is the common value of ψ_1 and ψ_2 in the untipped state. Equations (6.2) should suffice for the present purposes, where tipping angles are not expected to be large.

The classical Hamiltonian for dimer-tipping degrees of freedom on a Si(001) or Ge(001) surface may be written as follows:

$$H=\tfrac{1}{2}m\sum_{x,y}\{[\mathbf{v}(x,y,1)]^2+[\mathbf{v}(x,y,2)]^2\}+V(\{\theta(x,y)\}) \ . \tag{6.3}$$

Here $\theta(x,y)$ is the tipping angle for the dimer located on the surface by coordinates x,y, and V is the potential energy for the given surface state. The velocities $\mathbf{v}(x,y,1)$ and $\mathbf{v}(x,y,2)$ refer to the in-plane motions of atoms 1 and 2 for the dimer at surface location x,y, as illustrated in Fig. 14. The mass of an atom is m, which for the average isotopic composition of Si is

$$m=4.6510\times10^{-22}\ \text{g} \ . \tag{6.4}$$

The velocities appearing in the kinetic-energy portion of H, Eq. (6.3), have magnitudes equal to $b\dot{\psi}_1$ and $b\dot{\psi}_2$. After invoking the linear approximations (6.2), we thus obtain

$$H=\frac{ml^2}{4\cos^2\psi_0}\sum_{x,y}[\dot{\theta}(x,y)]^2+V(\{\theta(x,y)\}) \ . \tag{6.5}$$

Next, introduce the time, energy, and angle units τ_0, ε_0, and θ_0 so as to define the following reduced quantities:

$$\begin{aligned}&H^*=H/\varepsilon_0, \quad \Phi=V/\varepsilon_0 \ ,\\ &t^*=t/\tau_0, \quad \alpha(x,y)=\theta(x,y)/\theta_0 \ .\end{aligned} \tag{6.6}$$

Consequently, expression (6.5) for the Hamiltonian can be recast into the reduced form:

$$H^*=\frac{ml^2\theta_0^2}{4\varepsilon_0\tau_0^2\cos^2\psi_0}\sum_{x,y}\left[\frac{d\alpha(x,y)}{dt^*}\right]^2+\Phi(\{\alpha(x,y)\}) \ . \tag{6.7}$$

This replicates the form (3.1) used in the molecular-dynamics simulation provided that one chooses

$$\tau_0=\left[\frac{m}{2\varepsilon_0}\right]^{1/2}\left[\frac{l\theta_0}{\cos\psi_0}\right] \ . \tag{6.8}$$

Roberts and Needs[15] have reported pseudopotential total energy calculations for reconstructed Si(001) surfaces, whose results are useful in the present context. They find

$$\begin{aligned}l&=2.23\ \text{Å} \ ,\\ \psi_0&\cong55^\circ \ ,\end{aligned} \tag{6.9}$$

for the surface displaying a (2×1) symmetrical (unbuckled) dimer pattern. Their calculations indeed show that buckling reduces the surface energy slightly; the mean tipping angle θ_m [in a $p(2\times2)$ structure] was found to be

$$\theta_m=11.93^\circ \ . \tag{6.10}$$

If one accepts the standard case 1 as an acceptable dimensionless representation of Si(001), then θ_m would correspond to

$$\alpha_m=1.4451 \ . \tag{6.11}$$

Hence we must fix the angle unit at the value

$$\begin{aligned}\theta_0&=\theta_m/\alpha_m\\ &=8.256^\circ \ .\end{aligned} \tag{6.12}$$

Dimer-buckling energies represent small differences between large absolute energies. Consequently the corresponding quantum-mechanical calculations suffer from considerable uncertainty. Instead of using predicted buckling energies to fix the energy unit ε_0, we prefer instead to use an indirect estimate. In particular, the STM observations[8] for Si(001) suggest that a dimer-buckling phase transition exists between 120 K and room temperature. Using recent low-energy electron-diffraction (LEED) observations for guidance,[30] we assume that this transition occurs at 200 K. By identifying this point with the case 1 molecular-dynamics phase transition, T_m^* in

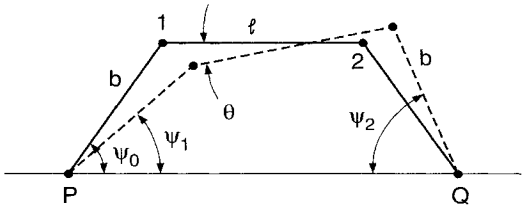

FIG. 14. Schematic mechanical linage used in assigning dimensions to the generic buckling model. Silicon atoms comprised in the dimer are denoted by 1 and 2, positions P and Q represent immobile substrate atoms.

Eq. (4.2), we conclude that

$$\epsilon_0 = k_B(200\ \text{K})/1.80$$
$$= 1.534\times 10^{-14}\ \text{erg}$$
$$= 9.574\ \text{meV} . \quad (6.13)$$

We can now proceed to evaluate time unit τ_0, utilizing results (6.4), (6.9), (6.12), and (6.13) for substitution into Eq. (6.8). One obtains

$$\tau_0 = 0.6898\ \text{ps} . \quad (6.14)$$

This assignment permits real-time interpretation of the autocorrelation functions in Figs. 7 and 8. As an example, the time intervals to the first minima appearing in Figs. 7 and 8 are 0.155 and 0.640 ps, respectively.

VII. DISCUSSION

The molecular-dynamics simulations reported herein unambiguously demonstrate that the generic dimer-buckling model defined in Sec. II (and originally in Ref. 1) has the capacity to undergo phase transitions. The simulations also establish that the presence, thermodynamic order, and temperature of those dimer-buckling phase transitions depend sensitively on the parameters of the model. The standard "case 1" set of parameter values, Eq. (3.3), has tentatively been suggested as a reasonable choice to describe the structurally perfect dimerized Si(001) surface, and appears to produce a weak first-order transition.

The LEED experiments for Si(001) by Tabata, Aruga, and Murata[30] appear to provide strong evidence for a dimer order-disorder transition at 200 K, and indeed we have used this temperature to fix the energy scale for our standard case 1 in the preceding Sec. VI. These authors interpret their observations as a "second-order order-disorder transition." In view of the extent of structural imperfection likely to be present in any real experiment, with a resulting smearing effect on any transition, it is certainly possible that a weakly first-order transition would occur after elimination of surface imperfections. In any case it is desirable to seek repetitions of at least LEED and STM observations vs temperature for a wide and controlled range of surface imperfections.

The theoretical literature contains several prior statistical-mechanical studies of dimer-buckling transitions on Si(001). Ihm *et al.*[31] have examined a spin-$\frac{1}{2}$ Ising model, with two-spin and four-spin interactions, using a renormalization-group approach. Saxena, Gawlinski, and Gunton[32] employed Monte Carlo simulation for the same model. Recently, Kochanski and Griffth[33] introduced a Ginsburg-Landau model, with coupling of dimers to surface electric fields such as those near STM tips. None of these approaches, however, has the capacity to yield a mechanically stable untipped dimer state, which is a characteristic feature of the present generic model.

Finally, it is worth stressing the apparent level of precision that quantum-mechanical calculations of surface energies will have to attain in order to a make reliable predictions about dimer-buckling phenomena. The units assignment of the preceding Sec. VI indicates that characteristic energies are of the order of 0.01 eV. Computational errors will have to be substantially lower, say 2–3 meV. Unfortunately this seems to be out of reach with present *ab initio* methods.

[1] F. H. Stillinger, Phys. Rev. B **46**, 9590 (1992).
[2] R. E. Schlier and H. E. Farnsworth, J. Chem. Phys. **30**, 917 (1959).
[3] J. J. Lander and J. Morrison, J. Chem. Phys. **37**, 729 (1962).
[4] T. D. Poppendieck, T. C. Ngoc, and B. M. Webb, Surf. Sci. **75**, 287 (1978).
[5] M. J. Cardillo and G. E. Becker, Phys. Rev. Lett. **40**, 1148 (1978).
[6] M. J. Cardillo and G. E. Becker, Phys. Rev. B **21**, 1497 (1980).
[7] R. J. Hamers, R. M. Tromp, and J. E. Demuth, Phys. Rev. B **34**, 5343 (1986).
[8] R. A. Wolkow, Phys. Rev. Lett. **68**, 2636 (1992).
[9] D. J. Chadi, Phys. Rev. Lett. **43**, 43 (1979).
[10] K. Pandey, in *Proceedings of the Seventeenth International Conference on the Physics of Semiconductors,* edited by D. J. Chadi and W. A. Harrison (Springer-Verlag, New York, 1985), p. 55.
[11] A. Redondo and W. A. Goddard III, J. Vac. Sci. Technol. **21**, 344 (1982).
[12] J. E. Northrup, Phys. Rev. Lett. **54**, 815 (1985).
[13] E. Artacho and F. Yndurain, Phys. Rev. Lett. **62**, 2491 (1989).
[14] M. C. Payne, N. Roberts, R. J. Needs, M. Needels, and J. D. Joannopoulis, Surf. Sci. **211**, 1 (1989).
[15] N. Roberts and R. J. Needs, Surf. Sci. **236**, 112 (1990).
[16] F. Jona, H. D. Smith, D. W. Jepson, and P. M. Marcus, J. Phys. C **12**, L455 (1979).
[17] S. D. Kevan and N. G. Stoffel, Phys. Rev. Lett. **53**, 702 (1984).
[18] H. J. Gossman, L. C. Feldman, and W. M. Gibson, Surf. Sci. **155**, 413 (1985).
[19] E. Fontes, J. R. Patel, and F. Comin, Phys. Rev. Lett. **70**, 2790 (1993).
[20] C. A. Lucas, C. S. Dower, D. F. McMorrow, G. C. L. Wong, F. J. Lamelas, and P. H. Fuoss, Phys. Rev. B **47**, 10 375 (1993).
[21] H. J. C. Berendsen and W. F. van Gunsteren, in *Molecular Dynamics Simulation of Statistical-Mechanical Systems,* edited by G. Ciccotti and W. G. Hoover (North-Holland, Amsterdam, 1986), pp. 52–55.
[22] T. L. Beck and R. S. Berry, in *The Physics and Chemistry of Small Clusters,* edited by P. Jena, B. K. Rao, and S. N. Khanna (Plenum, New York, 1987).
[23] J. D. Honeycutt and H. C. Andersen, J. Phys. Chem. **91**, 4950 (1987).
[24] F. H. Stillinger and D. K. Stillinger, J. Chem. Phys. **93**, 6013 (1990).
[25] F. H. Stillinger and T. A. Weber, Phys. Rev. A **28**, 2408 (1983).
[26] F. H. Stillinger and T. A. Weber, J. Phys. Chem. **91**, 4899 (1987).
[27] L. J. Root, J. Chem. Phys. **93**, 4364 (1990).
[28] H. Tanaka and K. Nakanishi, J. Chem. Phys. **95**, 3719 (1991).
[29] R. G. Della Valle and H. C. Andersen, J. Chem Phys. **97**, 2682

(1992).
[30]T. Tabata, T. Aruga, and Y. Murata, Surf. Sci. **179**, L63 (1987).
[31]J. Ihm, D. H. Lee, J. D. Joannopolis, and J. J. Xiong, Phys. Rev. Lett. **51**, 1872 (1983).
[32]A. Saxena, E. T. Gawlinski, and J. D. Gunton, Surf. Sci. **160**, 618 (1985).
[33]G. P. Kochanski, and J. E. Griffith, Surf. Sci. Lett. **249**, L293 (1991).